ELSEVIER

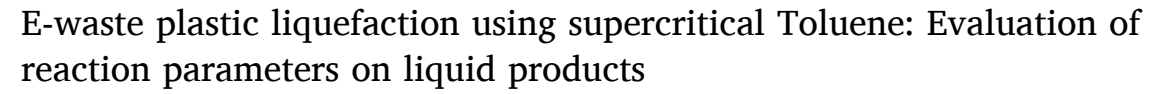
Contents lists available at ScienceDirect

# Waste Management

journal homepage: www.elsevier.com/locate/wasman



### Research Paper



Vahab Ghalandari, Hunter Smith, Adam Scannell, Toufiq Reza

Department of Chemistry and Chemical Engineering, Florida Institute of Technology, 150 West University Boulevard, Melbourne, FL 32901, USA



#### ARTICLE INFO

Keywords:
Electrical waste
Thermoplastics
Solvothermal liquefaction
Depolymerization
Toluene
Supercritical conditions

#### ABSTRACT

Solvothermal liquefaction (STL) is a thermochemical conversion technique that employs solvents other than water to transform waste plastics into valuable compounds. The objective of this study was to explore the potential use of supercritical toluene, a nonpolar solvent, for the depolymerization of four electrical waste (e-waste) thermoplastics, namely polyamide (PA), polycarbonate (PC), polyoxymethylene (POM), and polyether ether ketone (PEEK), into liquid products. Depolymerization experiments were carried out in batch reactors at three reaction temperatures (325, 350, and 375 °C), and three residence times (1, 3, and 6 h). The findings revealed that increasing STL temperature and extending the reaction time enhances the depolymerization of e-waste thermoplastics. The highest STL conversation (100 %) was observed for POM, and the lowest STL conversation (32.23 %) was observed for PEEK. Additionally, the ultimate analysis POM, and the liquid product obtained from STL at 375 °C and 6 h exhibited higher heating values (HHV) within the range of 31.43 to 35.31 MJ/kg. Thermogravimetric analysis (TGA) demonstrated that the boiling point distributions of liquid products are highly dependent on thermoplastic type. Finally, the reaction mechanisms of STL for PA, PC, POM, and PEEK were proposed based on gas chromatography-mass spectrometry (GCMS) analysis.

### 1. Introduction

Global production of thermoplastics reached nearly 400 million metric tons in 2020 and is projected to approach approximately 590 million metric tons by 2050 ("Global thermoplastic production by type, 2050," Statista.). Polycarbonate (PC), polyamide (PA), polyetheretherketone (PEEK), and polyoxymethylene (POM), are four types of thermoplastics commonly used in various electrical applications (Bagotia et al., 2018; Chen et al., 2021; Krause et al., 2009; X. Liu et al., 2022). PC is a strong and durable plastic that can withstand high impact and is often used in the production of electrical components such as switches, connectors, and housings due to its excellent electrical insulation properties and high-temperature resistance (Kim and Jo, 2009; Sung et al., 2006). PA, also known as nylon, is a lightweight plastic with high strength and abrasion resistance, commonly used in the production of electrical connectors, circuit breakers, and cable insulation due to its high strength, good electrical insulation properties, and resistance to abrasion and impact (Zhang et al., 2009; Zuev and Ivanova, 2012). PEEK is a high-performance thermoplastic with exceptional mechanical strength, high temperature resistance, and excellent chemical resistance (Santiago et al., 2021). PEEK is used in industries such as aerospace, automotive, electronics, and medical devices for components requiring strength, durability, and resistance to harsh environments (Rahman et al., 2016). POM, also known as acetal, is a low-friction and wear-resistant plastic widely employed in electrical applications because of its superb mechanical and electrical properties, making it a reliable and durable material for a wide range of electrical components (Mamunya et al., 2001; Zhao and Ye, 2011). Each of these thermoplastics possesses unique properties and is selected based on specific application requirements, contributing to their versatility and widespread use across various industries.

Despite all the advantages, these e-waste thermoplastics can also take hundreds of years to decompose in landfill, and their disposal can lead to pollution of the soil, air, and water (Mondal et al., 2019). Moreover, improper disposal of e-waste thermoplastics can also harm wildlife and cause health problems for humans (Kong et al., 2012). Recycling e-waste thermoplastics has several benefits, including minimizing waste disposal to landfills and reducing the environmental impact of e-waste thermoplastic (Preetam et al., 2023). However, the recycling process can be complicated because of the wide range of

E-mail address: treza@fit.edu (T. Reza).

<sup>\*</sup> Corresponding author.

plastic types and additives that are used in electronic devices, as well as the potential for contamination with hazardous materials (Asante et al., 2019; Zhang et al., 2012). The process of upcycling e-waste thermoplastic using thermochemical methods involves subjecting the plastic to high temperatures, breaking it down into its constituent parts that can subsequently be transformed into new materials (Jung et al., 2023). Thermochemical methods offer numerous advantages in the upcycling of e-waste thermoplastics. Initially, they enable the transformation of a diverse array of plastic materials into new products (Ghalandari et al., 2023), including those that are difficult to recycle through traditional mechanical or chemical methods (Capricho et al., 2022; Lee et al., 2023). Second, thermochemical methods can generate energy and valuable materials from waste, reducing the need for fossil fuels and virgin materials (Karimi Estahbanati et al., 2021). Finally, thermochemical methods can help to reduce the environmental impact of ewaste thermoplastic by diverting it from landfills and reducing greenhouse gas emissions (Alam et al., 2022; Lettieri and Al-Salem, 2011).

Among different thermochemical methods, solvothermal liquefaction (STL) using supercritical solvents is an emerging one (Azwar et al., 2023). STL is a chemical process that involves the conversion of solid biomass or plastic into valuable chemicals and liquid fuel using a solvent (Azwar et al., 2023; Su et al., 2022). The process typically occurs within a closed system, wherein the solid feedstock is combined with a solvent, and heated to temperatures ranging from 250 to 400 °C under high pressure (up to 200 bar) (Abdelraheem et al., 2023; Wądrzyk et al., 2023). Supercritical solvents have become increasingly popular in recent years due to their unique properties and numerous advantages (Faraz et al., 2022). One major advantage of using supercritical solvents is their high solvating power, which enables them to dissolve a wide range of compounds, including both polar and nonpolar substances (Park et al., 2021; Wang et al., 2019). Moreover, they can be performed at lower temperatures and pressures than traditional solvent processes, leading to reduced energy consumption and lower costs (Santana et al., 2012). Supercritical solvents are employed to provide a moderate reaction environment with improved mass and heat transport (Serrano et al., 2007). In recent years, numerous types of solvents have been evaluated for the STL process (Baloch et al., 2021b; Banivaheb et al., 2022; Ha Tran and Lee, 2020; Y. Liu et al., 2022; Riaz et al., 2018). One of the most commonly used solvents is either sub or supercritical water, or its combination with CO2 (Zhao et al. (2022)). This process is generally known as hydrothermal liquefaction (HTL). Plastics are less reactive than biomass even at temperatures when water is subcritical (Singh and Sharma, 2008). Additionally, HTL often leads to carbon loss in both aqueous and gaseous phases. Furthermore, the HTL process liquid must be appropriately treated before being discharged into the surrounding area (Mumtaz et al., 2023; Saha et al., 2022b). Methanol and acetone, as oxygenated solvents, were used in the STL process for plastic depolymerization (Y. Liu et al., 2022). The finding demonstrated that methanol and acetone depolymerize plastic more effectively than water (Banivaheb et al., 2022). Nevertheless, a previous investigation indicated that oxygenated solvents could be unsuitable for a variety of fuel-based usage (Brand et al., 2013). Using oxygenated solvents enhances the oxygen content in liquid product and boosts the cost of the process, which requires separation (Saha et al., 2022a). Alternatively, non-oxygenated solvents can be used for the STL of plastics. Recently, the STL of waste mixed plastics and waste polyurethane in toluene, which is a non-oxygenated solvent, was studied (Banivaheb et al., 2022; Ghalandari et al., 2022a). Toluene can donate hydrogen and has a lower critical temperature and pressure in comparison to water (Lee et al., 2005). Employing a hydrogen-donor solvent like toluene can substantially minimize the repolymerization reaction by stabilizing the generated free radicals (Sangon et al., 2006). Toluene, being a non-polar solvent, is an excellent option for applications requiring the extraction or separation of polar compounds from non-polar compounds. The nonpolar fraction of depolymerized plastic is readily dissolved in toluene, which can facilitate product separation (Saha et al., 2022a).

Supercritical toluene has a low viscosity, making it a good solvent for processes that require rapid mass transfer (Hutchenson et al., 1991; Lee et al., 2004). Overall, the advantages of using toluene as a non-oxygenated and non-polar solvent make it a suitable choice for a variety of applications such as STL process (Ghalandari et al., 2022a).

To the best of the authors' knowledge, just a few investigations have been carried out on the STL process of waste plastics using supercritical solvents (Baloch et al., 2021a, 2020; Banivaheb et al., 2022; Ghalandari et al., 2022a; Y. Liu et al., 2022; Saha et al., 2022a), but no research was identified by the authors covering STL of e-waste thermoplastics using supercritical toluene. To address this gap, the aim of the work was to study the possibility of using toluene in STL process of e-waste thermoplastic under supercritical conditions. In pursuit of this objective, the effect of STL temperature and residence time on STL conversion for types of e-waste thermoplastic (PA, PC, PEEK, and POM) was investigated. Subsequently, the liquid product resulting from the STL process was characterized to determine its potential applications. Conclusively, the study proposed the reaction mechanisms for each type of e-waste thermoplastic.

#### 2. Material and methods

#### 2.1. Materials

The four different types #7 thermoplastics (virgin plastics) includes polyamide (PA), polycarbonate (PC), polyoxymethylene (POM), and polyetheretherketone (PEEK) obtained from commercially accessible sources. The particle size, elemental analysis and proximate analysis of these thermoplastics are presented in the Supplementary File (Tables S1, and S2). The toluene with a purity of 99.5 % was purchased from Fisher Scientific (Waltham, MA, USA). The nitrogen gas (99.9 %), oxygen gas (99.9 %) and helium gas (99.9 %) were purchased from NexAir (Melbourne, FL, USA). The vanadium oxide ( $V_2O_5$ ) and 2,5-Bis (5-tert-butylbenzoxazol-2-yl) thiohene (BBOT) were purchased from Sigma-Aldrich (St. Louis, MO, USA).

## 2.2. Solvothermal liquefaction (STL) process

Custom-built stainless steel (SS-316) 7 mL custom reactors were used to carry out STL. The reactor vessels were brought to reaction temperature via a Techne SBL-2 sand bath (Vernon Hills, IL, USA). In the experiments, a specific plastic to toluene mass ratio of 1:10 was utilized. This resulted in the combination of 0.5 g of plastic with 5 g of toluene for each test. Each plastic, under three reaction temperatures (325, 350, and 375 °C), was also subjected to three residence times of 1, 3, and 6 h. After STL reaction, the reactor vessels were cooled via natural convection. The choice to examine the range of reaction temperature (325 to 375 °C) and residence time (1 to 6 h) at three different points was based on our previous well-considered experimental studies (Saha et al., 2022a; Banivaheb et al., 2022; Ghalandari et al., 2022a). Following cooling to ambient temperature, the vessels were then opened under the lab hood to vent the gas, and the solution product was filtered through a syringe filter with a pore size of 1.0 µm. This filtration process allowed for the separation of the liquid and solid phases. The solid mass was subsequently calculated after the solid residue was subjected to oven drying at 105  $^{\circ}\text{C}.$  The weight of the gas produced during the STL trial was determined by measuring the weight of the reactor vessel after loading it with feedstock and toluene before the trial, and then weighing it again after venting the gas following the trial.

Due to the constraints of the custom reactors, analyzing the gaseous products proved unfeasible. Therefore, further analysis was exclusively performed on the liquid products. To this end, all the filtered liquid products were carefully collected and stored in glass vials. These vials were promptly refrigerated to ensure the preservation of the liquid samples until the analysis could be conducted. Toluene was not recovered because the primary focus of this study was the investigation of the

liquefaction process, its conditions, and the resulting liquid product, while the recovery and recycling of toluene were considered beyond the scope of this specific research, which aimed to comprehend the fundamental aspects of the process and its impact on plastic depolymerization. Each experiment was performed two times, and the values presented in the manuscript are the averages of these replicates. The schematic diagram of STL process steps are illustrated in Fig. 1. The STL conversion, solid residue yield, gas yield, and liquid product yield were calculated employing Eqs. (1)–(4).

$$STL conversion(\%) = (1 - \frac{weight of dried solid residue after STL}{weight of feeds to ck}) \times 100\% \hspace{0.5cm} \textbf{(1)}$$

$$Solidresidue yield (\%) = (\frac{weight of dried solidresidue after STL}{weight of feed stock}) \times 100\% \tag{2}$$

$$Gasyield(\%) = (\frac{weightofgas}{weightoffeedstock}) \times 100\%$$
(3)

$$Liquidproductyield(\%) = 100 - Solidyield(\%) - Gasyield(\%)$$
 (4)

#### 2.3. Characterization of STL liquid products

Liquid products underwent elemental analysis via a Thermo Scientific Flash 1112 Organic Elemental Analyzer (Waltham, MA, USA) (Saha et al., 2022a). Once the toluene was dried off, the liquid products were mixed with a vanadium oxide conditioner. Standards for the CHNS analyzer were prepared with BBOT being utilized as a calibration standard and  $\rm V_2O_5$  again as a conditioner. The samples were combusted in the elemental analyzer's furnace at 950 °C in ultra-high purity oxygen and with a helium carrier gas. The oxygen content was found by means of a difference method (Quaid et al., 2022). The Dulong formula (Eq. (5) was utilized to determine the higher heating value (HHV) of liquid product (Hosokai et al., 2016).

$$HHV\left(\frac{MJ}{Kg}\right) = 0.3383C + 1.422(H - \frac{O}{8})$$
 (5)

where C, H, and O are the wt.% of carbon, hydrogen, and oxygen

respectively, determined from the elemental analysis. Please note that that the HHV is reported as ash-free.

The STL liquid product's boiling point distribution was determined via a Perkin Elmer TGA 4000 (Waltham, MA, USA) (Saha et al., 2022a). Under a nitrogen environment (flow of 20 mL/min), the liquid product was first heated from ambient temperature to 115 °C and held isothermally for 5 min to eliminate any excess toluene present in the samples. Then, at a continuous rate of 20 °C/min, the sample was heated from 115 to 600 °C, and were held isothermally for 5 min at 600 °C. It should be noted that only liquid components with boiling points higher than 115 °C (the boiling point of toluene) were considered, and any components with boiling points below this temperature were not included.

FTIR analysis of liquid products was performed with a Nicolet 6700 FTIR Spectrophotometer (Waltham, MA, USA). A total of 64 scans with a spectra wavelength of 500–4000 cm<sup>-1</sup>, were taken at a resolution of 4, which allowed for analysis of the functional groups in the STL liquid products. With the STL solvent being toluene, a background of toluene was implemented via placing a droplet of it onto the IR card before adding the liquid product (Ghalandari et al., 2022b).

Gas Chromatography-Mass spectroscopy was implemented via a 5975 Mass Spectrometric detector coupled with an Agilent 7890 GC. A Supelco Equity 1701 column was also equipped with the GC. The gas input was held steadily at 250  $^{\circ}\text{C}$  with a splitting ratio of 1:1 and the helium flowed at 5 mL/min. The oven was heated up for 4 min to a temperature of 45  $^{\circ}\text{C}$ , and then further heated to reach 280  $^{\circ}\text{C}$  for 20 min. Excluding any overlap chromatogram peaks, prior to injection, the samples were doped with an (n-decane, 99 %) solution (0.1 wt%). Compounds were identified by comparing data to the NIST mass spectral database.

#### 3. Results and discussion

### 3.1. STL conversion of e-waste thermoplastic

Fig. 2a illustrates the STL conversion of PA, PC, PEEK, and POM at different STL process conditions. The given data in Fig. 2a consists of three temperature and conversion data sets for PA, PC, PEEK, and POM at three residence times: 1, 3, and 6 h. The temperature values are 325,

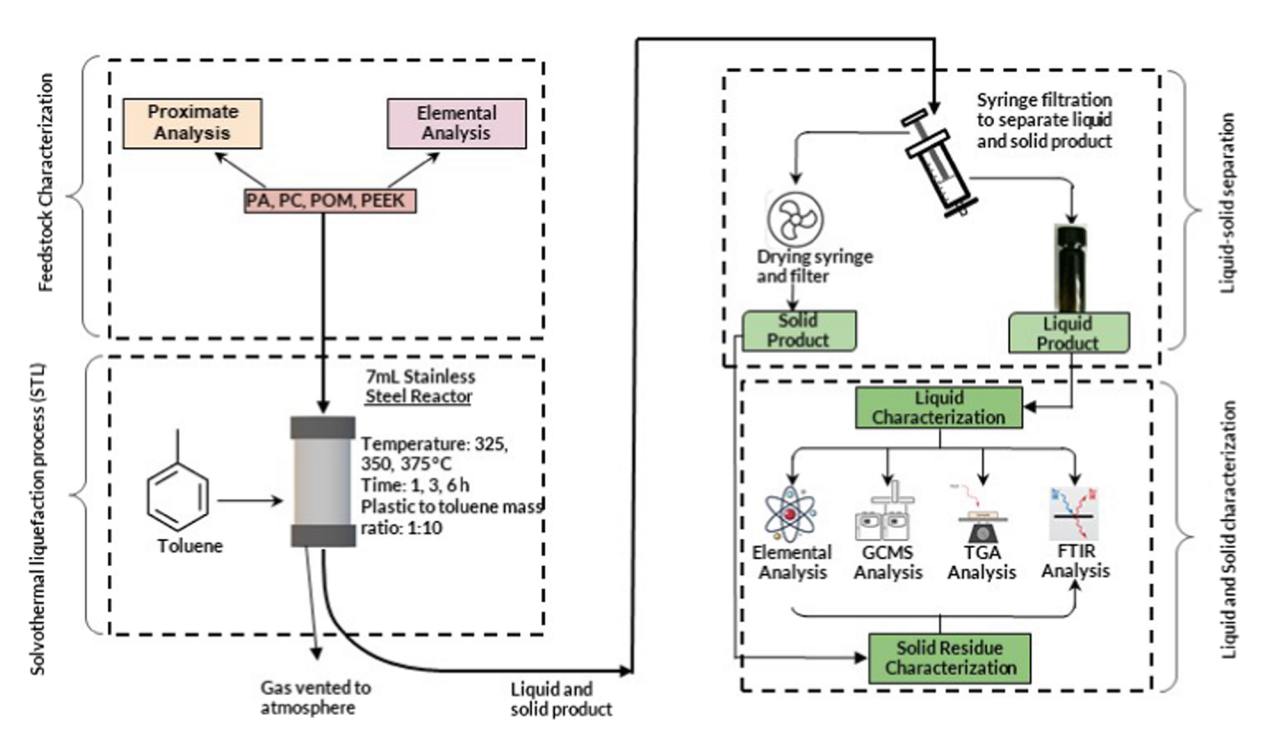
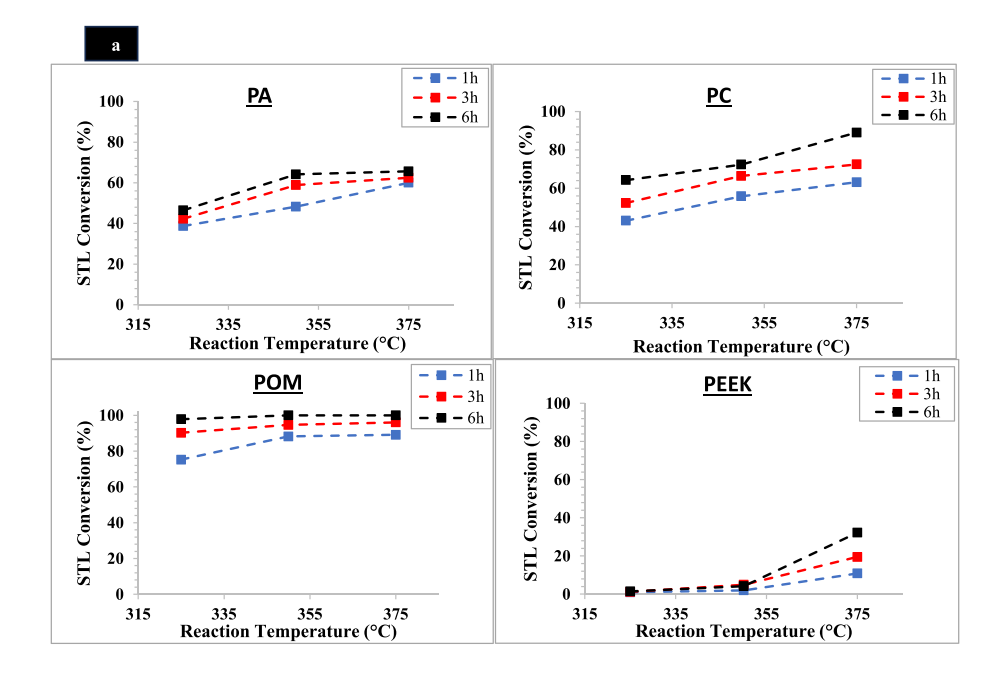


Fig. 1. Schematic diagram of Solvothermal liquefaction of e-waste plastics.



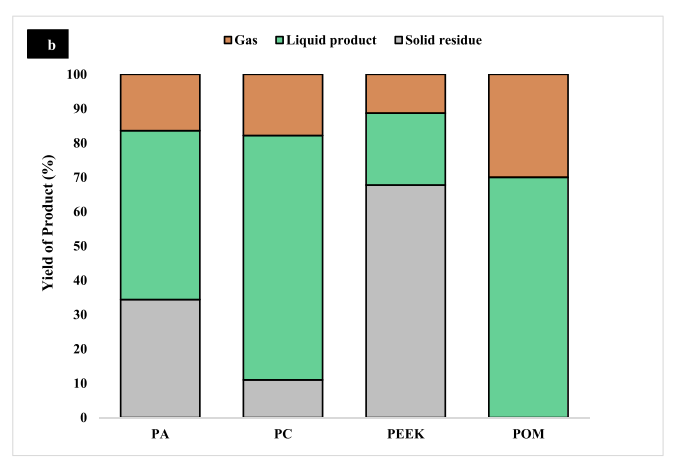


Fig. 2. (2a) The effect of reaction temperature and residence time on the STL conversion of PA, PC, POM, and PEEK. (2b) Variation of product fraction yields (wt.%) from STL using toluene by e-waste thermoplastics type (375 °C, 6 h).

350, and 375 °C, and the corresponding STL conversion values of PA for the 1 h residence time are 38.72, 48.25, and 60.01 %, for the 3 h residence time are 42.3, 58.85, and 62.44 %, and for the 6 h residence time are 46.46, 64.12, and 65.62 %. These data suggest that as the temperature increases, the conversion of PA also tends to increase. One study (Seshasayee and Savage, 2020a) reported the positive effect of reaction temperature on the conversion rate of polypropylene and polystyrene for HTL. Additionally, the conversion values for the 1 h residence time are lower than those for the 3 and 6 h residence times, suggesting that longer residence times lead to higher conversion rates. As the residence time increases, more of the plastic molecules have an opportunity to come into contact with the solvent, allowing for more depolymerization to occur (Dement'ev et al., 2019). This is because the solvent molecules can penetrate into the plastic and break the polymer chains (Baloch et al., 2021b).

From Fig. 2a, it can be observed that as the temperature increases, the STL conversion of PC tends to increase. Additionally, as the residence time increases, the STL conversion also tends to increase. Specifically, for PC, at a residence time of 1 h, the STL conversion increases from 43.04 % at 325 °C to 63.11 % at 375 °C. At a residence time of 3 h, the STL conversion increases from 52.25 % at 325 °C to 72.41 % at 375 °C. Finally, at a residence time of 6 h, the STL conversion increases

from 64.21 % at 325 °C to 89.01 % at 375 °C. The higher STL conversion rate at 375 °C may be the result of extensive depolymerization reactions that break down the solid phase into smaller liquid product molecules. This is because higher temperatures can increase the mobility of the polymer chains and make them more susceptible to breaking apart in the presence of the solvent (Murthy, 2006; Xu et al., 2021).

Based on the result (Fig. 2a), the STL conversion of PEEK at 325 and 350 °C is negligible (less than 5 %). The conversion of PEEK 375 °C increases from 10.85 % for 1 h to 32.23 % for 6 h. It shows that the depolymerization of PEEK happens at a high temperature (375 °C). However, in comparison with PA and PC, the depolymerization of PEEK in toluene through STL is low. Depolymerization of PEEK in a solvent can be challenging for several reasons. First, PEEK has a high degree of crystallinity, which means that the polymer chains are densely packed and closely linked, making it harder for the solvent to access the polymer chains and break them apart (Mehmet-Alkan and Hay, 1993). Second, PEEK has strong intermolecular forces, which can make it difficult for the solvent molecules to penetrate into the polymer matrix and break the polymer chains (Kurtz, 2012). Third, PEEK has a high melting temperature of around 343 °C, which means that it is a highly stable polymer and requires high temperatures to initiate depolymerization (Wu et al., 2014).

It can also be observed in Fig. 2a that the conversion of POM increases by raising temperature. Furthermore, as the residence time is increased, the conversion rate tends to approach 100 %. Specifically, the conversion rates for POM at a residence time of 1 h, increase from 75.25 % at 325 °C to 89.1 % at 375 °C. At a residence time of 3 h, the conversion rates increase from 90.25 % at 325 °C to 96.05 % at 375 °C. Finally, at a residence time of 6 h, the conversion rates increase from 97.87% at 325 °C to 100% at both 350 °C and 375 °C. It is worth noting that the conversion rates for POM are quite high, with conversion rates of over 90 % at a residence time of 3 h even at lower temperatures. Depolymerization of POM in the STL process is high for several reasons. First, POM has a lower melting temperature (175 °C) than some other thermoplastic polymers, such as PEEK, which means that it can be depolymerized at lower temperatures (Chen et al., 2008). Second, POM has weaker intermolecular forces compared to other thermoplastic polymers, such as PEEK. The intermolecular forces between polyoxymethylene molecules are primarily due to van der Waals forces, which are weak (Gray and McCRUM, 1971). This makes the polymer chains more susceptible to depolymerization in the presence of a suitable solvent. Finally, POM is less thermally stable compared to some other thermoplastic polymers, such as PEEK. This means that it can be depolymerized more easily under milder reaction conditions (Archodoulaki

The production yields of STL at 375 °C and 6 h for PA, PC, POM, and PEEK are illustrated in Fig. 2b. PA results in a solid residue yield of 34.38 %, with a notable liquid product yield of 49.22 % and a gas yield of 16.41 %. It indicates that a significant portion of the PA is converted into oil and gas. PC, on the other hand, shows a lower solid residue yield of 10.99 % and a high liquid product yield of 71.21 %, with a gas yield of 17.80 %. PC is more readily converted into liquid product, making it a promising feedstock for maximizing liquid product production. POM distinguishes itself with a 0 % solid residue yield, indicating complete conversion into other products. It primarily yields liquid product (70 %) and gas (30 %), highlighting its high reactivity during STL process using toluene. In contrast, PEEK has the highest solid residue yield at 67.77 %, with a lower liquid product yield of 20.95 % and a gas yield of 11.28 %. PEEK is the least reactive among the four materials, leaving a significant solid residue.

In Table 1, the production yield results of this study at  $350\,^{\circ}\text{C}$  for  $1\,\text{h}$  are presented, alongside recent non-catalytic solvothermal plastic studies. These detailed production yield and operating condition data assist researchers in making informed decisions regarding feedstock selection and process optimization, aligning with their specific goals, whether it involves maximizing oil production, minimizing solid residue, or achieving other desired outcomes for various applications.

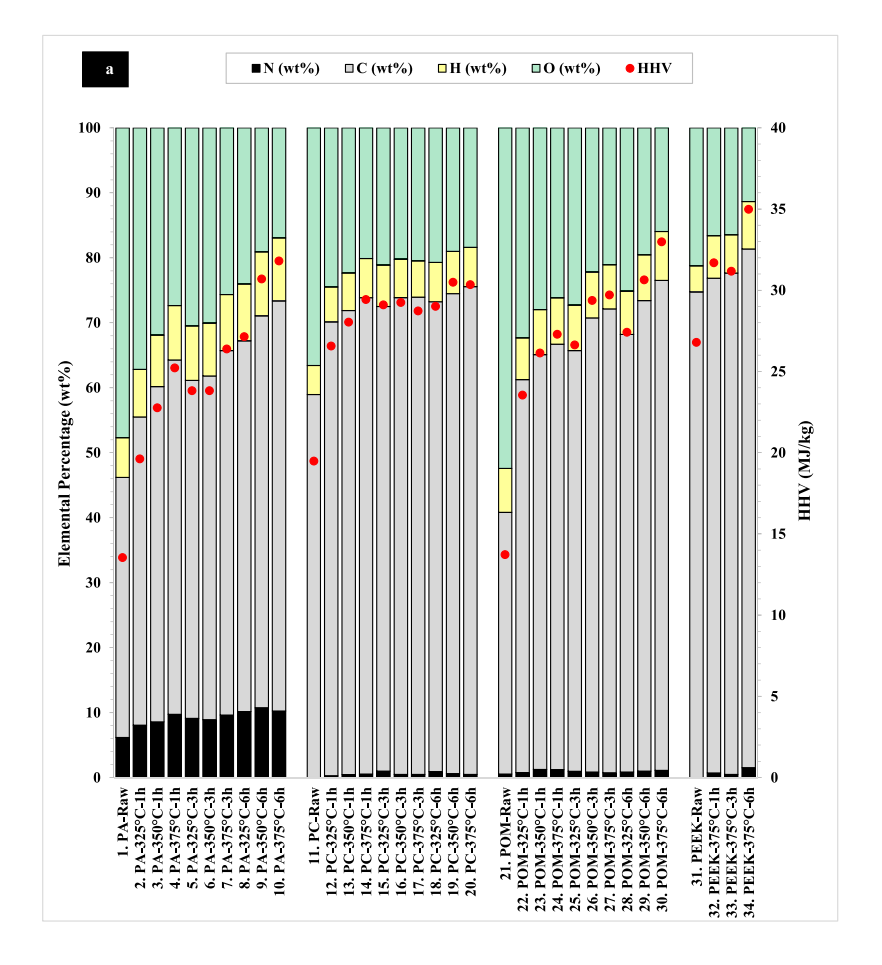
#### 3.2. Elemental analysis of STL liquid products

Fig. 3a shows the range of carbon, hydrogen, and nitrogen content in four different types of raw e-waste thermoplastic and liquid product samples. PA liquid product has the lowest carbon content, while PEEK liquid product has the highest carbon content. PA liquid product has the lowest carbon and highest hydrogen content, while PEEK liquid product and PC liquid product have the highest carbon, and lowest hydrogen content, respectively. Furthermore, PA liquid product has a significant amount of nitrogen (between 8.07 wt% and 10.73 wt%), while PC, PEEK and POM have a small amount of nitrogen. Based on the results, the carbon content of liquid product samples is significantly higher than the carbon content of raw thermoplastics, and the oxygen content of liquid product samples is significantly less than the oxygen content of raw thermoplastics. Similar finding was observed when toluene was used as solvent in STL of polyurethane, polypropylene, polystyrene, and polyurethane (Ghalandari et al., 2022a; Saha et al., 2022a). The reason might be the breakdown of the polymer chains and the release of volatile hydrocarbons during STL process. These hydrocarbons are then condensed and recovered as liquid product, which has a higher carbon content compared to the feedstocks (Baek et al., 2004; Keane, 2009). Generally, when reaction time and residence time is increased, the carbon content of liquid product samples increases, and oxygen content of liquid product samples decreases. A similar trend were observed for STL of e-waste plastics using methanol and acetone as solvents (Y. Liu et al., 2022). The increase in carbon content of liquid product samples with increasing temperature of solvothermal reaction can be attributed to the thermal cracking of the feedstocks because the formation of smaller hydrocarbon molecules through thermal cracking can increase in higher temperature (Angyal et al., 2007; Chandrasekaran et al., 2015). The longer residence time allows for more extensive cracking reactions to take place, resulting in a greater conversion of the feedstocks to liquid product and an overall increase in the carbon content of the liquid product sample (Chandrasekaran et al., 2015; Hussein et al., 2021).

Fig. 3b displays a Van Krevelen diagram (Li et al., 2022) for STL liquid product samples. The data presented shows the changes in O/C and H/C atomic ratios of STL liquid product samples under different operational conditions, and highlights the variations observed in comparison to the raw thermoplastics. The O/C atomic ratio reflects the level of oxygenation of the liquid product (Lee et al., 2013), while the H/C atomic ratio reflects the level of hydrogenation (Saxby, 1980). These ratios are used to determine the quality of liquid product, its thermal stability, and its potential as a feedstock for various processes such as refining, upgrading, and conversion into value-added products (Chen et al., 2016; Lu et al., 2018). The raw PA has an O/C atomic ratio of 0.89 and an H/C atomic ratio of 1.82, and although the O/C atomic ratio of

**Table 1**Product distribution in the current STL study and recent plastic STL studies.

Feedstock	Solvent	Temperature (°C)	Residence Time (min)	Solvent-to-Plastic (gram) Ratio	Solid residue (wt%)	Liquid product (wt%)	Gas (wt %)	Reference
Polyamide	Toluene	350	60	10	51.75	36.19	12.06	Current study
Polycarbonate	Toluene	350	60	10	44.22	44.62	11.16	Current study
Polyoxymethylene	Toluene	350	60	10	11.80	61.74	20.46	Current study
Polyetheretherketone	Toluene	350	60	10	98.03	1.28	0.69	Current study
Polyethylene	Acetone	350	90	5	24.66	39.33	36.01	(Liu et al., 2022a)
Polyethylene	Methanol	350	90	5	33.51	15.22	48.73	(Liu et al., 2022b)
Polyethylene	Water	350	90	5	97.74	0	2.26	(Liu et al., 2022)
Polystyrene	Ethanol	350	60	1	4.42	82.23	13.35	(Ahmad et al., 2020)
Rubber	Methanol	350	30	1	5.67	18.42	75.91	(Ahmad et al., 2023)
Polycarbonate	Water	350	60	17	4.33	24.87	70.8	(Seshasayee and Savage, 2020a)
Polystyrene	Water	350	60	17	3.54	78.52	17.94	(Seshasayee and Savage, 2020a)
Polypropylene	Water	350	60	17	81.52	1.42	82.94	(Seshasayee and Savage, 2020a)



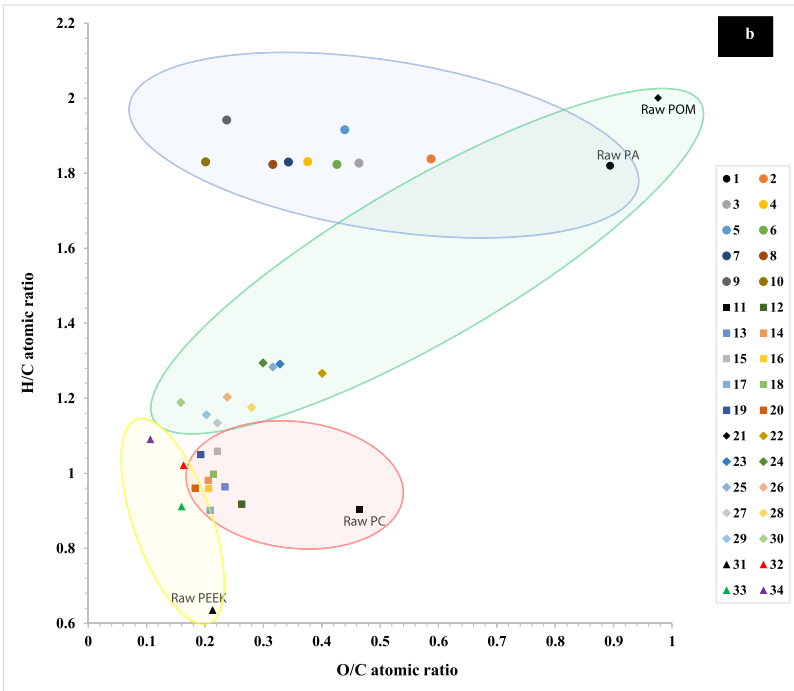


Fig. 3. (3a) Elemental composition, and HHV of the STL liquid products and raw e-waste thermoplastics. (3b) Van Krevelen diagram of STL liquid products generated at different process conditions (the numbers in this figure refer to experiment numbers in Fig. 3a).

PA liquid products is less than that of raw PA, the H/C atomic ratio of liquid products is similar to that of raw PA. The raw PC has an O/C atomic ratio of 0.47 and an H/C atomic ratio of 0.9, and while the O/C atomic ratio of PC liquid products is lower than that of raw PC, the H/C atomic ratio of liquid products is slightly higher than that of raw PC. The raw POM has an O/C atomic ratio of 0.98 and an H/C atomic ratio of 2, and while the O/C atomic ratio of POM liquid products is lower than that of raw POM, the H/C atomic ratio of liquid products is significantly less than that of raw POM. The raw PEEK has an O/C atomic ratio of 0.21 and an H/C atomic ratio of 0.64, and while the O/C atomic ratio of PEEK liquid products is slightly lower than that of raw PEEK, the H/C atomic ratio of liquid products is higher than that of raw PEEK. Earlier studies demonstrated that the H/C and O/C atomic ratios significantly correlate with the type of plastics. For example, a previous research (Seshasayee and Savage, 2020a) discovered that whereas HTL of polyethylene terephthalate creates a liquid product with lower O/C and higher H/C atomic ratios than the feedstocks, HTL of polypropylene provides a liquid product with greater  $\rm O/C$  and lower  $\rm H/C$  atomic ratios than the raw material.

The HHVs of liquid products, which are calculated based on elemental analysis, are illustrated in Fig. 3a. The estimation of the Higher Heating Value (HHV) of crude oil in this study is crucial for assessing the energy content and potential recovery from liquefied ewaste plastic products, essential for evaluating their feasibility as an energy source or feedstock. The HHV of liquid products is significantly higher than the HHV of raw thermoplastics. The HHV value for PA liquid product HHV is between 19.61 and 31.80 MJ/kg, for PC liquid product is between 26.56 and 30.34 MJ/kg, for POM liquid product is between 23.54 and 32.98 MJ/kg, and for PEEK liquid product is between 31.69 and 34.98 MJ/kg. The reason is that the STL process reduces the oxygen content of raw thermoplastic by breaking it and converting it to liquid product with low oxygen content, and high carbon content (Azwar et al.,

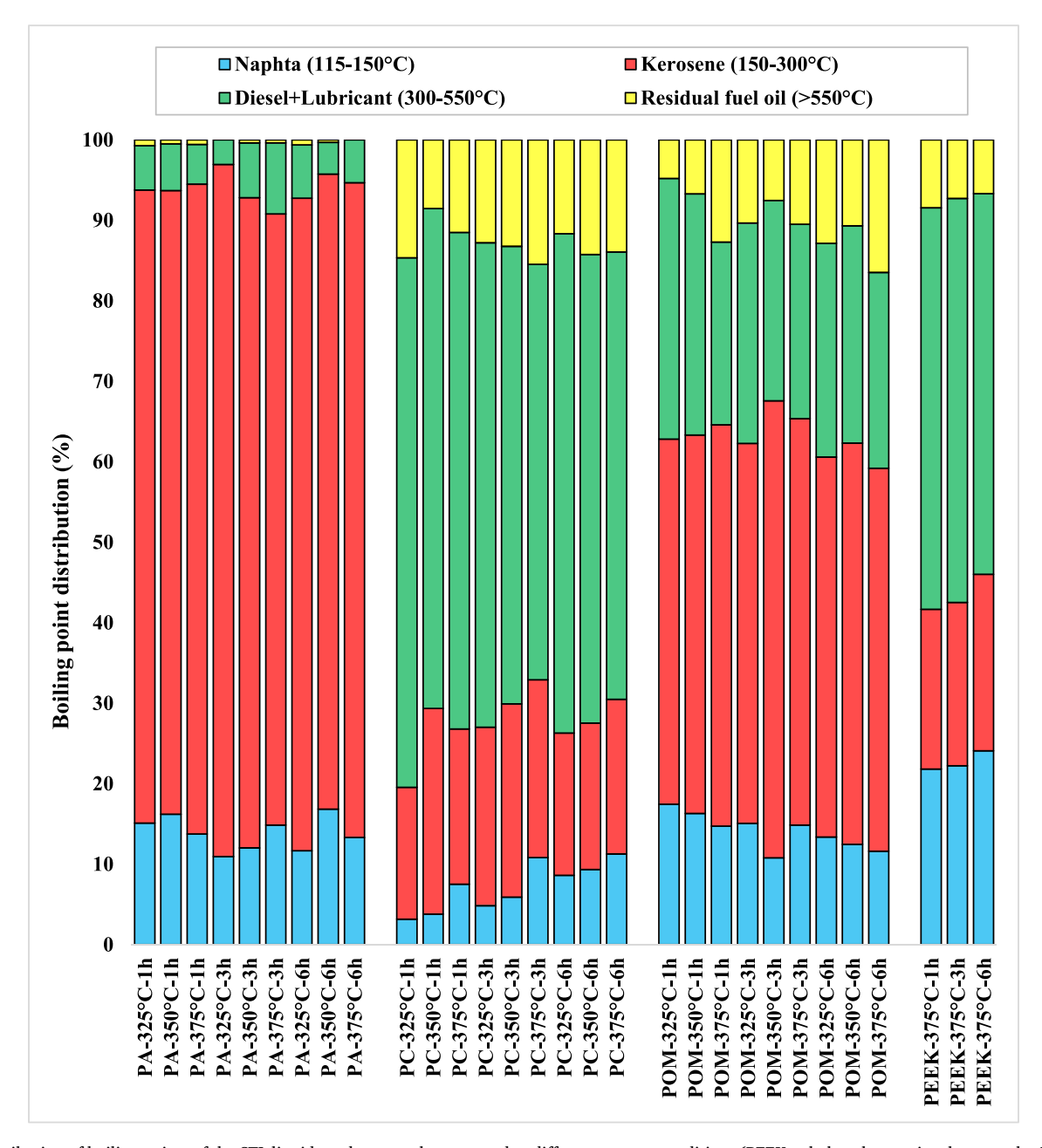


Fig. 4. Distribution of boiling points of the STL liquid product samples prepared at different process conditions (PEEK only has three points because the STL of PEEK at 325 and 350 °C resulted in negligible liquid product).

2023; Y. Liu et al., 2022). The previous STL study in supercritical toluene demonstrated that the HHV of mixed plastic's mixed plastic is between 30 and 37 MJ/kg (Saha et al., 2022a). Overall, by increasing reaction temperature, and residence time, the HHV of liquid product samples increases. The reason is that the carbon and hydrogen contents in liquid product increase by deoxygenation mechanism during the STL process, resulting in the production of liquid products with a higher HHV (Y. Liu et al., 2022; Saha et al., 2022a). In overall, the data suggests that these four types of liquid product differ in their chemical composition, with variations in carbon, hydrogen, and nitrogen content that may have implications for their processing and use in various applications.

### 3.3. Boiling point distribution of STL liquid products

The liquid product from STL of thermoplastics comprises so many different compounds, therefore, the boiling temperatures for various combinations vary (Y. Liu et al., 2022). TGA was used to measure weight loss of the liquid product as the temperature gradually rises. Fig. 4 shows the data by displaying the weight-percent loss of each liquid product at various temperature ranges corresponding to boiling point cuts in refinery products.

The naphtha weight percentages of produced liquid products are as follows: PA liquid product ranges from 10.94 % to 16.83 %, PC liquid product ranges from 3.16 % to 11.25 %, POM liquid product ranges from 11.61 % to 17.45 %, and PEEK liquid product ranges from 21.82 % to 24.09 %. It can be observed that PEEK liquid product has the highest naphtha weight percentage, followed by POM liquid product and PA liquid product. PC liquid products have the lowest naphtha weight percentage range. PA liquid product exhibits the highest kerosene weight percentage range, ranging from 75.94 % to 81.35 %. Following PA liquid product, POM liquid product has the second-highest range, varying from 45.36 % to 56.80 %. PEEK liquid product falls in the middle with a narrower range of 19.85 % to 21.94 %. PC liquid product has the lowest kerosene weight percentage range, ranging from 16.4 % to 25.57 %. PC liquid product has the highest diesel and lubricant weight percentage range, ranging from 51.64 % to 65.79 %. PEEK liquid product follows with a range of 47.3 % to 50.2 %, indicating a relatively high proportion of diesel and lubricant. POM liquid product falls in the middle with a range of 22.73 % to 32.4 %. PA liquid product has the lowest diesel and lubricant weight percentage range, ranging from 3.06 % to 8.82 %. These ranges indicate the varying amounts of diesel and lubricant components present in each liquid product type. POM liquid product exhibits the highest residual fuel oil weight percentage range. ranging from 4.79 % to 16.48 %. PC liquid products follow with a range of 8.54 % to 15.45 %, indicating a relatively high proportion of residual fuel oil. PEEK liquid product falls in the middle with a narrower range of 6.66 % to 8.43 %. PA liquid product has the lowest residual fuel oil weight percentage range, ranging from 0 % to 0.72 %. These ranges represent the varying amounts of residual fuel oil present in each liquid product type, with POM and PC liquid products having the highest content and PA liquid product having the lowest.

The reason for the variation in naphtha, kerosene, diesel, and lubricant weight percentages among different liquid products is mainly due to differences in their chemical compositions and sources. Different types of liquid products have varying proportions of hydrocarbons and other components, which results in variations in naphtha, kerosene, diesel, and lubricant content. One study (Seshasayee and Savage, 2020b) also reported the significant effect of the type of plastic on the proportion of hydrocarbons in plastic liquid product, which is in line with this study. Finally, a specific relation between STL temperature/residence time and the proportion of hydrocarbons is not observed from TGA results in Fig. 4.

### 3.4. The FTIR of STL liquid products

FTIR of liquid products can provide valuable information about its

chemical bonding. As shown in Fig. 5, the PA liquid product sample, the peak at  $732~{\rm cm}^{-1}$  is attributed to C–H bending vibrations in aromatic compounds (Nava et al., 1996), while the peaks at  $1145~{\rm cm}^{-1}$  and  $1193~{\rm cm}^{-1}$  corresponds to C–O stretching vibrations (Stuart and Sutherland, 2004). The peak at  $1550~{\rm cm}^{-1}$  corresponds to N–O stretching (Hadjiivanov et al., 1994), and at  $2613~{\rm cm}^{-1}$  corresponds to N–H in nitrogen compounds (Tripp and Hair, 1993). The peak at  $1645~{\rm cm}^{-1}$  is attributed to C = C stretching vibrations in conjugated aromatics. The peak at  $2952~{\rm cm}^{-1}$  corresponds to C–H stretching vibrations in alkanes (Kim and Kang, 2012).

In the case of the PC liquid product samples, the peak at  $683 \, \mathrm{cm}^{-1}$  is attributed to C–H bending vibrations in aromatic compounds, while the peak at  $893 \, \mathrm{cm}^{-1}$  corresponds to C–H bending vibrations in alkanes (Nava et al., 1996). The peak at  $1275 \, \mathrm{cm}^{-1}$  corresponds to CH<sub>2</sub> bending vibrations, and the peak at  $1411 \, \mathrm{cm}^{-1}$  corresponds to C–H bending vibrations in aromatic compounds (Matos et al., 1992). The peak at  $1579 \, \mathrm{cm}^{-1}$  is attributed to C = C stretching vibrations in aromatics, while the peak at  $1643 \, \mathrm{cm}^{-1}$  corresponds to C = C stretching vibrations in conjugated aromatics (Shibagaki et al., 2001). The peak at  $1716 \, \mathrm{cm}^{-1}$  is due to C = O stretching vibrations in phenol compounds (Yang et al., 2013). Finally, the peak at  $2960 \, \mathrm{cm}^{-1}$  is due to C–H stretching vibrations in alkenes and aromatics (Kim and Kang, 2012).

As can be seen in Fig. 5, the POM liquid product sample, the peak at  $696~\mathrm{cm}^{-1}$  is associated with C–H bending vibrations in alkanes (Nava et al., 1996). The peak at  $728~\mathrm{cm}^{-1}$  corresponds to the wagging mode of CH<sub>2</sub> groups (Nava et al., 1996), and the peak at  $1145~\mathrm{cm}^{-1}$  is due to C–O stretching vibrations in aliphatic ether (Stuart and Sutherland, 2004). The peak at  $1193~\mathrm{cm}^{-1}$  is attributed to C–O bending vibrations in oxygen compounds like phenol (Stuart and Sutherland, 2004), while the peak at  $1495~\mathrm{cm}^{-1}$  corresponds to C–C stretching vibrations in aromatics. Finally, the peak at  $3023~\mathrm{cm}^{-1}$  is due to C–H and CH<sub>2</sub> stretching vibrations in alkenes and aromatics (Kim and Kang, 2012).

In the case of the PEEK liquid product sample, the peak at  $691 \text{ cm}^{-1}$  is attributed to C–H bending vibrations in aromatic compounds (Nava et al., 1996), while the peak at  $1014 \text{ cm}^{-1}$  corresponds to C–O bending vibrations (Ahmed Ismail et al., 2022). The peak at  $1194 \text{ cm}^{-1}$  corresponds to C–O bending vibrations in oxygen compounds (Stuart and Sutherland, 2004). The peak at  $1496 \text{ cm}^{-1}$  is attributed to C–C stretching vibrations in aromatics, while the peak at  $1590 \text{ cm}^{-1}$  corresponds to C = C stretching vibrations in conjugated aromatics. The peak at  $1749 \text{ cm}^{-1}$  is due to C = O stretching vibrations in aromatic compounds (Yang et al., 2013). Finally, the peak at  $3021 \text{ cm}^{-1}$  is attributed to C–H and CH<sub>2</sub> stretching vibrations in alkenes and aromatics (Kim and Kang, 2012).

### 3.5. Chemical composition of STL liquid products

GCMS was utilized to specify the molecular components in the STL liquid product samples for each of the four thermoplastic types at high temperature (375 °C) for different residence times, and the results were presented in Fig. 6 and Tables S3-S14 (Supplementary file). In the liquid product, the components were divided into four main types: aliphatic hydrocarbons, aromatic hydrocarbons, oxygen containing compounds, and nitrogen containing compounds. Due to the polymers used in the experiment not containing a pure carbon backbone, there is not a significant number of aliphatic groups in the liquid product (Li et al., 2002), with only the POM group containing any noticeable percentage of aliphatic compounds.

When the PA underwent STL, the major components produced are caprolactam, o-xylene, p-xylene, ethylbenzene, cyclopentanone, and 3,5-dimethyl phenol. Caprolactam is the major nitrogen containing chemical in the liquid product and composed 47 % and 48 % of the liquid product in the 1 and 3 h residence times respectively. Caprolactam is a significant product due to it being used in the production of PA through a ring opening polymerization mechanism (Oh et al., 2019;

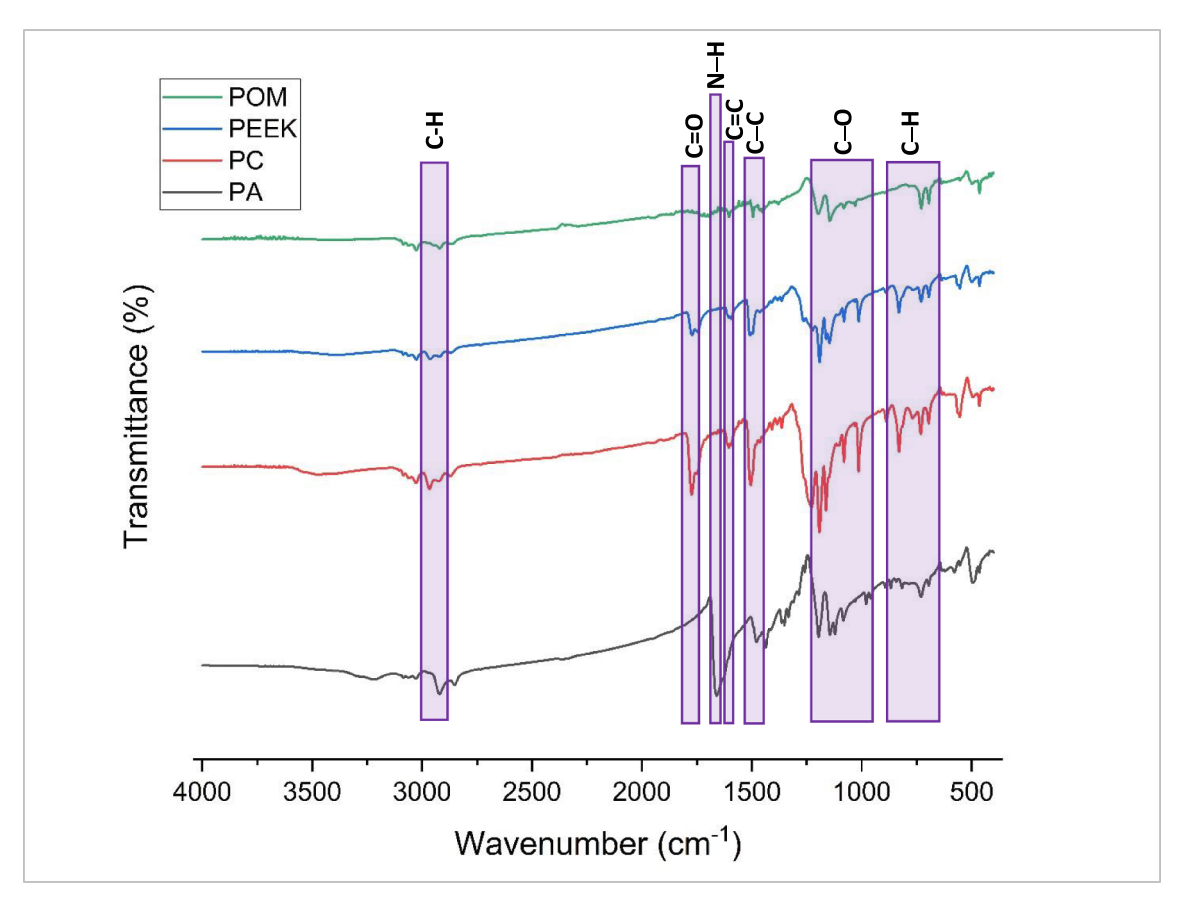


Fig. 5. FTIR spectra of STL liquid products obtained at 375  $^{\circ}\text{C}$  and 6 h.

Vicard et al., 2017). The percentage of caprolactam dropped significantly to 26.8 % during the 6 h residence time. The drop in the caprolactam percentage is likely caused from the caprolactam degrading at a slow rate during the process (Scelia et al., 1967), the result of which appears at longer residence times.

The GCMS data of PC liquid product show that it consists of only aromatic and oxygen containing compounds. The oxygen containing components primarily of phenols and the concentration of oxygenated compounds increase from 35.7 % at 1 h to 64.8 % at 3 h and decreases to 29.5 % at 6 h. This trend is likely caused by the PC still being degraded into phenols between 1 and 3 h during STL, and the formation of phenols likely slows down past the 3 h mark phenol is likely to degrade after some time under high temperature and pressure(Iurascu et al., 2009); therefore, the concentration of phenol will decrease if the residence time is significantly high.

The STL of POM has a much higher variety of compounds produced with there being approximately 32 compounds produced in the 6 h trial that composed of less than 1 % of the total area. Another thing that makes it difficult for POM to be characterized is the presence of nitrogen in the range of 12–26 % in the liquid product, while the typical structure of POM does not have any nitrogen (Carazzolo and Mammi, 1963; Carazzolo, 1963). As such, it is likely that there are chemical additives to the structure such as a crosslinker or coating. Based on the formation of altretamine in the liquid product, it is likely that the POM uses the melamine formaldehyde based crosslinking mechanism in order to structurally strengthen the POM and that is the source of the nitrogen within the compounds(Hu et al., 2006).

PEEK is typically more degradation resistant than PC and will take a longer time to degrade under similar conditions (Liao et al., 2020; Martin et al., 2003). Based on the GCMS data, at residence time of 1 h, most of the oxygenated compounds is benzaldehyde, which consists of 22 % of the total product. The benzaldehyde is then shown to degrade

over time, with only 13.8 % of benzaldehyde remaining at 3 h, and 1.1 % remaining at 6 h. While the benzaldehyde is degrading, phenol is forming, resulting in the total amount of oxygenated compounds increasing from residence times of 3 h (13.8 %) to 6 h (47 %).

### 3.6. Proposed STL reaction mechanisms

As seen in Fig. 7a, the primary purpose of toluene in the reaction mixture is to serve as a hydrogen donor to the components to prevent further degradation of the components via beta scission or homolysis. This hydrogen abstraction reaction is expected to occur due to the appearance of bibenzyl in the reaction mixture, which would most reasonably be formed by the combination reaction between two toluene radicals. Toluene would be particularly effective at this due to having a high presence of tertiary carbon atoms along with a resonance structure to stabilize the toluene radical, meaning that the toluene radical would likely be more stable than the radicals formed during the degradation process. This process is expected to run in parallel to methyl cleavage, in which the toluene loses its methyl group to thermolysis (Pamidimukkala et al., 2002). This reaction is demonstrated by the presence of methyl substituted toluene groups in the PEEK degradation product, which are unlikely to form via PEEK degradation due to the lack of methyl groups within the PEEK structure.

The most significant result of the PA degradation was the significant formation of caprolactam in the liquid product (Fig. 7b). This fits with most pyrolysis-based studies on PA degradation, as the heterolysis of the amide bonds throughout the polymer can give way to the formation of caprolactam through a ring closing mechanism, functionally being the inverse of most common PA synthesis methods (Zakharyan and Maksimov, 2022). Under a significant longer reaction time, the caprolactam will decompose, resulting in lower caprolactam formation in the final product. The formation of cyclopentanone in each of the products is

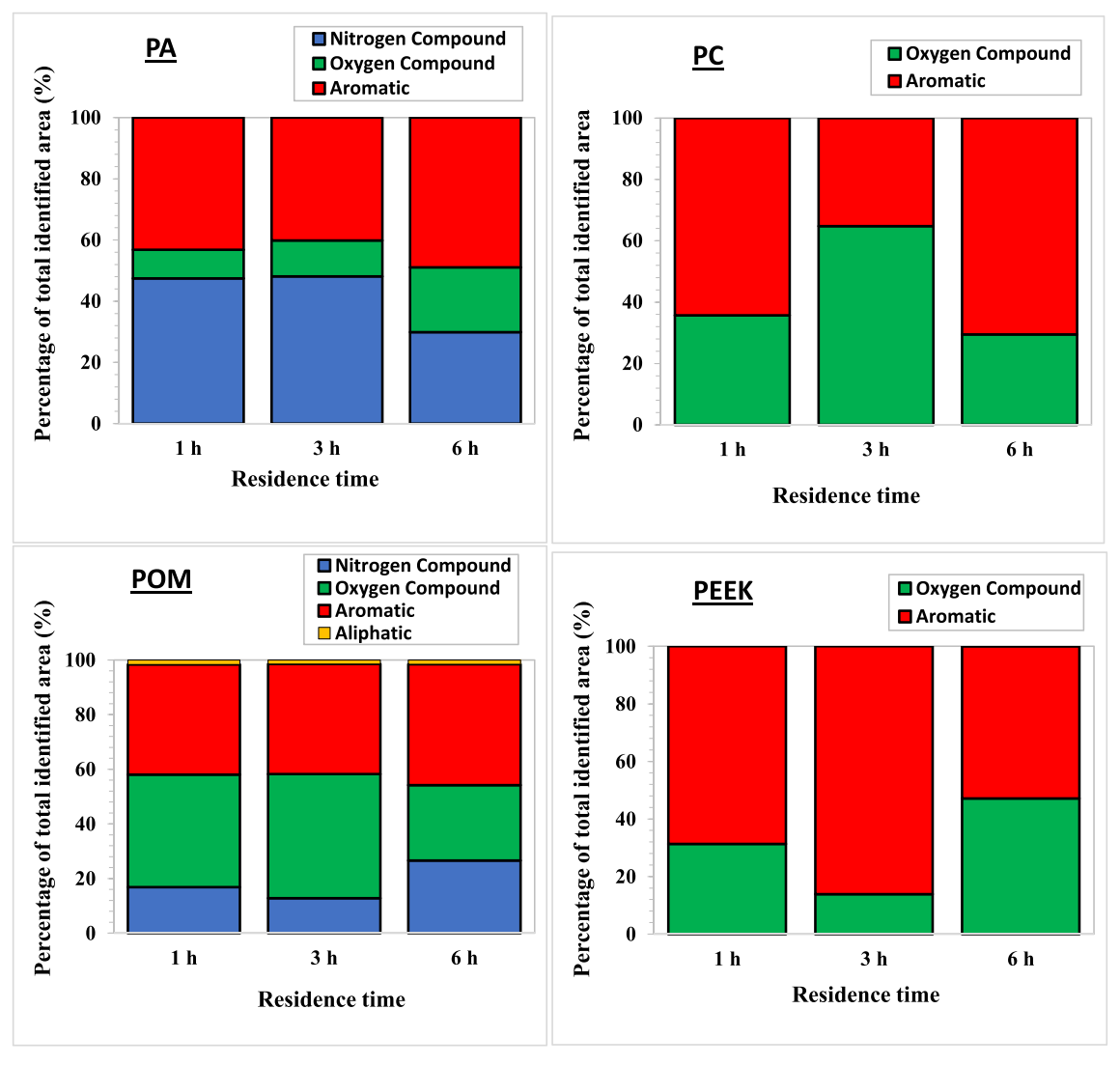


Fig. 6. Total identified area of different chemical compounds presents in the STL liquid products at 375 °C.

likely based on a similar mechanism, with the thermolysis of bonds resulting in radical formation that can undergo radical recombination on its poles to form a ring. The formation of the dimethyl benzyl groups is likely to be formed by reactions between the toluene radicals formed in the reaction and methyl radicals formed by thermolysis of methyl groups.

The degradation of PC with toluene results in the formation of primarily substituted benzyl groups (Fig. 7c). This fits with most literature as reactions at these temperatures and pressures are unlikely to break aromatic compounds and the degradation would rather start at the linkage molecules in this compound, being the quaternary carbon and the carbonate linkage (Wan et al., 2021). The partial degradation can be seen by the formation of 4-(2-Phenyl-2-propanyl) phenol in the liquid product, which is a direct decomposition of the bisphenol A (BPA) component. The formation of the methyl substituted toluene in the liquid product is likely from the thermolysis of the methyl groups on the quaternary carbon in the BPA component followed by hydrogen abstraction and radical combination of the methyl group and the toluene solvent. The phenol groups are direct decomposition products of BPA, as seen in Fig. 7c.

The typical degradation mechanism for POM is to have an unzipping reaction along the chain after the initial lysis to for formaldehyde (Kusy and Whitley, 2005). The formaldehyde can react with radical benzyl groups to form benzaldehyde (Fig. 7d). Outside of Formaldehyde,

another initial decomposition product is likely to be methyl formate. Methyl formate and toluene appear to be the precursor of a significant amount of the liquid product, including 2-phenylethyl ester acetic acid and 2-phenylethyl ester benzeneacetic acid. There is also a significant amount of nitrogen containing compounds within the liquid feed, which is likely due to the crosslinking agent containing nitrogen.

For the STL process of PEEK, it is expected that the polymer degradation to begin via scission of the weaker linkage bonds between the aromatic rings (Patel et al., 2010). The formation of benzaldehyde in the liquid product can be seen on the left of Fig. 7e. The ketone linkage is cleaved via thermolysis and then the resulting radicals are quenched via hydrogen abstraction with toluene. Similarly, phenols are generated via the same mechanism except the initial thermolysis reaction is with the ether bonds. The formation of 3,5-dimethyl-phenol on the liquid product can be explained via the substitution of the phenol with the methyl groups formed from the toluene thermolysis. The use of toluene in the solvent is beneficial in prevention of the production of fluorenone in the liquid product, as without the presence of a hydrogen donor, diradical benzyl groups can combine to form fluorenone (Perng et al., 1999).

# 4. Conclusions

In this study, solvothermal liquefaction (STL) of four types of e-waste thermoplastics (PA, PC, POM, and PEEK) were performed using

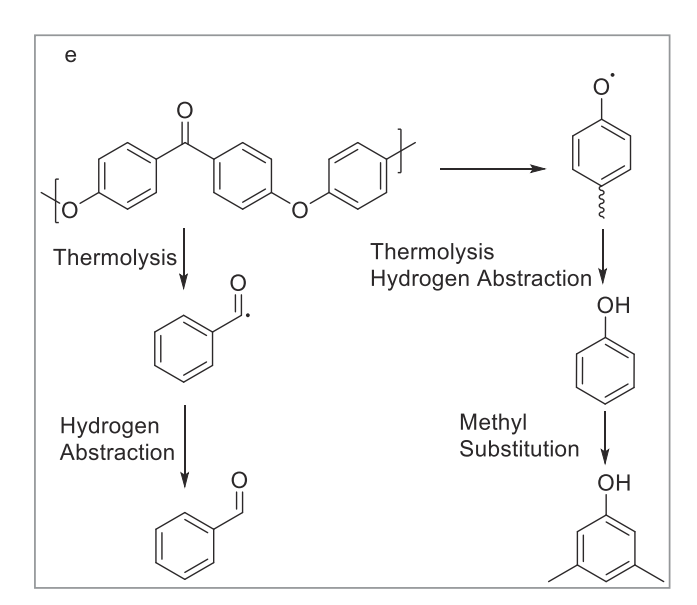


**Fig. 7.** (7a) Purpose of Toluene in Degradation Process (R represents radicals that are formed during STL), (7b) proposed reaction mechanism for PA degradation, (7c) proposed reaction mechanism for PC degradation, (7d) proposed reaction mechanism for POM degradation, and (7e) proposed reaction mechanism for PEEK degradation.

supercritical toluene. The results indicated the significant impact of temperature and residence time on the solvothermal liquefaction (STL) conversion of thermoplastics. For instance, at 375 °C, PA's conversion increases from 60.01 % (1 h) to 65.62 % (6 h), while PC's conversion rises from 43.04 % to 89.01 %. In contrast, PEEK exhibits minimal conversion at 325 °C and 350 °C, emphasizing its high thermal stability. On the other hand, POM shows consistent high conversion rates, reaching 100 % at 375 °C and 6 h, owing to its lower melting temperature and weaker intermolecular forces. STL liquid products, produced at higher temperatures (375 °C) and longer residence times (6 h), exhibited the following HHV values:  $PA - 31.80 \, MJ/kg$ ,  $PC - 30.34 \, MJ/kg$ kg, POM - 32.98 MJ/kg, and PEEK - 34.98 MJ/kg. The boiling temperatures of most portions of liquid products were in the range of boiling temperature of naphtha (115-150 °C), kerosene (150-300 °C), and diesel/lubricant (300-550 °C). The FTIR analysis revealed the presence of aromatics and oxygen compounds in all liquid products. GCMS analysis demonstrated that the presence of significant amount of nitrogen components in PA, and PC liquid products. Moreover, a small number of aliphatic components were detected in PC liquid products. In summary, the results showed that STL process using supercritical toluene is a significant method for upcycling e-waste thermoplastic to produce liquid product. The result of this work can be used to design a thermochemical process for upcycling thermoplastic.

**Author Contributions:** Conceptualization, V.G. and T.R.; Data Curation, V.G.; Formal Analysis, V.G. and A.S.; Writing—original draft, V.G., H.S. and A.S.; Writing—review and editing, T.R.; Funding acquisition, T.R.; Project administration, T.R. All authors have read and agreed to the published version of the manuscript.

#### **Funding**

The material is based upon work partially supported by National Science Foundation under Grant No. 2123495.

# CRediT authorship contribution statement

Vahab Ghalandari: Conceptualization, Data curation, Formal analysis, Writing – original draft. Hunter Smith: Writing – original draft. Adam Scannell: Formal analysis, Writing – original draft. Toufiq Reza: Conceptualization, Writing – review & editing, Project administration.

### **Declaration of competing interest**

The authors declare that they have no known competing financial interests or personal relationships that could have appeared to influence the work reported in this paper.

### Data availability

Data will be made available on request.

### Acknowledgments

The authors acknowledge Mr. Andrew Wagner from Mainstream Engineering Corporation for his assistance with GCMS analysis. The authors also acknowledge Ms. Marjan Asemani from Florida Institute of Technology for her assistance with reaction mechanisms.

### Appendix A. Supplementary data

Supplementary data to this article can be found online at https://doi.org/10.1016/j.wasman.2023.11.027.

#### References

- Abdelraheem, A.M., Abdel-Rahim, M.A., Hamad, D., Abd-Elnaiem, A.M., 2023. Physical characterizations and methane gas-sensing of AlxZn1-xO nanoparticles. Appl. Surf. Sci. 619, 156729 https://doi.org/10.1016/j.apsusc.2023.156729.
- Ahmad, N., Ahmad, N., Maafa, I.M., Ahmed, U., Akhter, P., Shehzad, N., Hussain, M., 2020. Thermal conversion of polystyrene plastic waste to liquid fuel via ethanolysis. Fuel 279, 118498. https://doi.org/10.1016/j.fuel.2020.118498.
- Ahmad, N., Ahmad, N., Ahmed, U., Jameel, A.G.A., Hussain, M., Arif, M.M., 2023. Production of fuel oil from elastomer rubber waste via methanothermal liquefaction. Fuel 338, 127330. https://doi.org/10.1016/j.fuel.2022.127330.
- Ahmed Ismail, K., El Askary, A., Farea, M.O., Awwad, N.S., Ibrahium, H.A., Eid Moustapha, M., Menazea, A.A., 2022. Perspectives on composite films of chitosan-based natural products (Ginger, Curcumin, and Cinnamon) as biomaterials for wound dressing. Arab. J. Chem. 15, 103716 https://doi.org/10.1016/j.arabjc.2022.103716.
- Alam, S.S., Husain Khan, A., Khan, N.A., 2022. Plastic waste management via thermochemical conversion of plastics into fuel: a review. Energy Sources Part A 44, 1–20. https://doi.org/10.1080/15567036.2022.2097750.
- Angyal, A., Miskolczi, N., Bartha, L., 2007. Petrochemical feedstock by thermal cracking of plastic waste. Journal of Analytical and Applied Pyrolysis, PYROLYSIS 2006: Papers presented at the 17th International Symposium on Analytical and Applied Pyrolysis, Budapest, Hungary, 22-26 May 2006 79, 409–414. https://doi.org/ 10.1016/j.jaap.2006.12.031.
- Archodoulaki, V.-M., Lüftl, S., Seidler, S., 2006. Oxidation induction time studies on the thermal degradation behaviour of polyoxymethylene. Polym. Test. 25, 83–90. https://doi.org/10.1016/j.polymertesting.2005.08.011.
- Asante, K.A., Amoyaw-Osei, Y., Agusa, T., 2019. E-waste recycling in Africa: risks and opportunities. Current Opinion in Green and Sustainable Chemistry. Special Issue on Africa Green Solvents 18, 109–117. https://doi.org/10.1016/j.cossc.2019.04.001.
- Azwar, E., Mahari, W.A.W., Liew, R.K., Ramlee, M.Z., Verma, M., Chong, W.W.F., Peng, W., Ng, H.S., Naushad, M.u., Sonne, C., Lam, S.S., 2023. Remediation and recovery of Kariba weed as emerging contaminant in freshwater and shellfish aquaculture system via solvothermal liquefaction. Sci. Total Environ. 876, 162673 https://doi.org/10.1016/j.scitotenv.2023.162673.
- Baek, K.-H., Kim, H.-S., Oh, H.-M., Yoon, B.-D., Kim, J., Lee, I.-S., 2004. Effects of Crude Oil, Oil Components, and Bioremediation on Plant Growth. J. Environ. Sci. Health A 39, 2465–2472. https://doi.org/10.1081/ESE-200026309.
- Bagotia, N., Choudhary, V., Sharma, D.K., 2018. A review on the mechanical, electrical and EMI shielding properties of carbon nanotubes and graphene reinforced polycarbonate nanocomposites. Polym. Adv. Technol. 29, 1547–1567. https://doi. org/10.1002/pat.4277.
- Baloch, H.A., Siddiqui, M.T.H., Nizamuddin, S., Mubarak, N.M., Khalid, M., Srinivasan, M.P., Griffin, G.J., 2020. Solvothermal co-liquefaction of sugarcane bagasse and polyethylene under sub-supercritical conditions: Optimization of process parameters. Process Saf. Environ. Prot. 137, 300–311. https://doi.org/ 10.1016/j.psep.2020.01.018.
- Baloch, H.A., Siddiqui, M.T.H., Nizamuddin, S., Mubarak, N.M., Khalid, M., Srinivasan, M.P., Griffin, G.J., 2021a. Catalytic co-liquefaction of sugarcane bagasse and polyethylene for bio-oil production under supercritical conditions: Effect of catalysts. J. Anal. Appl. Pyrol. 153, 104944 https://doi.org/10.1016/j. jaan.2020.104944.
- Baloch, H.A., Siddiqui, M.T.H., Nizamuddin, S., Riaz, S., Haris, M., Mubarak, N.M., Griffin, G.J., Srinivasan, M.P., 2021b. Effect of solvent on hydro-solvothermal co liquefaction of sugarcane bagasse and polyethylene for bio-oil production in ethanol-water system. Process Saf. Environ. Prot. 148, 1060–1069. https://doi.org. 10.1016/j.psep.2021.02.015.
- Banivaheb, S., Ghalandari, V., Smith, H., Reza, M.T., 2022. SolvX: Solvothermal conversion of mixed waste plastics in supercritical toluene in presence of Pd/C catalyst. J. Environ. Chem. Eng. 10, 108622 https://doi.org/10.1016/j. iong.2022.108622
- Brand, S., Susanti, R.F., Kim, S.K., Lee, H., Kim, J., Sang, B.-I., 2013. Supercritical ethanol as an enhanced medium for lignocellulosic biomass liquefaction: Influence of physical process parameters. Energy 59, 173–182. https://doi.org/10.1016/j. energy.2013.06.049.
- Capricho, J.C., Prasad, K., Hameed, N., Nikzad, M., Salim, N., 2022. Upcycling Polystyrene. Polymers 14, 5010. https://doi.org/10.3390/polym14225010.
- Carazzolo, G.A., 1963. Structure of the normal crystal form of polyoxymethylene. J. Polym. Sci., Part A: Gen. Pap. 1, 1573–1583. https://doi.org/10.1002/pol.1963.100010510.
- Carazzolo, G., Mammi, M., 1963. Crystal structure of a new form of polyoxymethylene. J. Polym. Sci., Part A: Gen. Pap. 1, 965–983. https://doi.org/10.1002/ pol/10621.0001031
- Chandrasekaran, S.R., Kunwar, B., Moser, B.R., Rajagopalan, N., Sharma, B.K., 2015. Catalytic Thermal Cracking of Postconsumer Waste Plastics to Fuels. 1. Kinetics and Optimization. Energy Fuels 29, 6068–6077. https://doi.org/10.1021/acs. energyfuels.5b01083.
- Chen, C.-S., Chen, S.-C., Liaw, W.-L., Chien, R.-D., 2008. Rheological behavior of POM polymer melt flowing through micro-channels. Eur. Polym. J. 44, 1891–1898. https://doi.org/10.1016/j.eurpolymj.2008.03.007.
- Chen, D., Yu, X., Song, C., Pang, X., Huang, J., Li, Y., 2016. Effect of pyrolysis temperature on the chemical oxidation stability of bamboo biochar. Bioresour. Technol. 218, 1303–1306. https://doi.org/10.1016/j.biortech.2016.07.112.
- Chen, C., Zhao, X., Ye, L., 2021. Polyoxymethylene/Carbon Nanotube Self-Assembly Networks with Improved Electrical Conductivity for Engineering Functional

- Structural Materials. ACS Appl. Nano Mater. 4, 9606–9615. https://doi.org/10.1021/acsanm.1c02022.
- Dement'ev, K.I., Palankoev, T.A., Alekseeva, O.A., Babkin, I.A., Maksimov, A.L, 2019. Thermal depolymerization of polystyrene in highly aromatic hydrocarbon medium. J. Anal. Appl. Pyrol. 142, 104612 https://doi.org/10.1016/j.jaap.2019.05.001.
- Faraz, O., Poustchi, M., Nazari Denyani, E., Movahedi, P., Rajabi Kouchi, F., Shahriari, R., 2022. Thermodynamic modeling of pharmaceuticals solubility in pure, mixed and supercritical solvents. J. Mol. Liq. 353, 118809 https://doi.org/10.1016/ j.molliq.2022.118809.
- Ghalandari, V., Banivaheb, S., Peterson, J., Smith, H., Reza, M.T., 2022a. Solvothermal liquefaction of waste polyurethane using supercritical toluene in presence of noble metal catalysts. AIChE J 68, e17863.
- Ghalandari, V., Smith, H., Volpe, M., Messineo, A., Reza, T., 2022b. Effect of Acidic Hydrochar on Plastic Crude Oil Produced from Hydrothermal Liquefaction of Waste PVC. Processes 10, 2538. https://doi.org/10.3390/pr10122538.
- Ghalandari, V., Volpe, M., Codignole Lùz, F., Messineo, A., Reza, T., 2023. Role of acidic hydrochar on dechlorination of waste PVC in high temperature hydrothermal treatment and fuel properties enhancement of solid residues. Waste Manag. 169, 125–136. https://doi.org/10.1016/j.wasman.2023.07.005.
- Global thermoplastic production by type 2050 [WWW Document], n.d. . Statista. URL https://www.statista.com/statistics/1192886/thermoplastics-production-volumeby-type-globally/ (accessed 5.21.23).
- Gray, R.W., McCRUM, N.G., 1971. Orientation in Rolled Polyoxymethylene. Nat. Phys. Sci. 234, 117–118. https://doi.org/10.1038/physci234117a0.
- Ha Tran, M., Lee, E., 2020. Development and optimization of solvothermal liquefaction of marine macroalgae Saccharina japonica biomass for biopolyol and biopolyurethane production. J. Ind. Eng. Chem. 81, 167–177. https://doi.org/ 10.1016/j.jiec.2019.09.005.
- Hadjiivanov, K., Bushev, V., Kantcheva, M., Klissurski, D., 1994. Infrared spectroscopy study of the species arising during nitrogen dioxide adsorption on titania (anatase). Langmuir 10, 464–471. https://doi.org/10.1021/la00014a021.
- Hosokai, S., Matsuoka, K., Kuramoto, K., Suzuki, Y., 2016. Modification of Dulong's formula to estimate heating value of gas, liquid and solid fuels. Fuel Process. Technol. 152, 399–405. https://doi.org/10.1016/j.fuproc.2016.06.040.
- Hu, Y., Ye, L., Zhao, X., 2006. Synthesis of the melamine–formaldehyde polycondensate and its thermal stabilization effect on polyoxymethylene. Polymer 47, 2649–2659. https://doi.org/10.1016/j.polymer.2006.02.050.
- Hussein, Z.A., Shakor, Z.M., Alzuhairi, M., Al-Sheikh, F., 2021. Thermal and catalytic cracking of plastic waste: a review. Int. J. Environ. Anal. Chem. 1–18. https://doi. org/10.1080/03067319.2021.1946527.
- Hutchenson, K.W., Roebers, J.R., Thies, M.C., 1991. Fractionation of petroleum pitch with supercritical toluene. The Journal of Supercritical Fluids, Proceedings of the Symposium on Supercritical Fluids 4, 7–14. https://doi.org/10.1016/0896-8446(91) 90025-2
- Iurascu, B., Siminiceanu, I., Vione, D., Vicente, M.A., Gil, A., 2009. Phenol degradation in water through a heterogeneous photo-Fenton process catalyzed by Fe-treated laponite. Water Res. 43, 1313–1322. https://doi.org/10.1016/j.watres.2008.12.032.
- Jung, H., Shin, G., Kwak, H., Hao, L.T., Jegal, J., Kim, H.J., Jeon, H., Park, J., Oh, D.X., 2023. Review of polymer technologies for improving the recycling and upcycling efficiency of plastic waste. Chemosphere 320, 138089. https://doi.org/10.1016/j. chemosphere.2023.138089.
- Karimi Estahbanati, M.R., Kong, X.Y., Eslami, A., Soo, H.S., 2021. Current Developments in the Chemical Upcycling of Waste Plastics Using Alternative Energy Sources. ChemSusChem 14, 4152-4166. https://doi.org/10.1002/cssc.202100874.
- Keane, M.A., 2009. Catalytic Transformation of Waste Polymers to Fuel Oil. ChemSusChem 2, 207–214. https://doi.org/10.1002/cssc.200900001.
- Kim, K.H., Jo, W.H., 2009. A strategy for enhancement of mechanical and electrical properties of polycarbonate/multi-walled carbon nanotube composites. Carbon 47, 1126–1134. https://doi.org/10.1016/j.carbon.2008.12.043.
- Kim, B.-J., Kang, K.-S., 2012. Fabrication of a Crack-Free Large Area Photonic Crystal with Colloidal Silica Spheres Modified with Vinyltriethoxysilane. Cryst. Growth Des. 12, 4039–4042. https://doi.org/10.1021/cg3005147.
- Kong, S., Liu, H., Zeng, H., Liu, Y., 2012. The Status and Progress of Resource Utilization Technology of e-waste Pollution in China. Procedia Environmental Sciences, The Seventh International Conference on Waste Management and Technology (ICWMT 7) 16, 515–521. https://doi.org/10.1016/j.proenv.2012.10.071.
- Krause, B., Pötschke, P., Häußler, L., 2009. Influence of small scale melt mixing conditions on electrical resistivity of carbon nanotube-polyamide composites. Composites Science and Technology, CNT-NET 07 Special Issue with regular papers 69, 1505–1515. https://doi.org/10.1016/j.compscitech.2008.07.007.
- Kurtz, S.M., 2012. Chapter 1 An Overview of PEEK Biomaterials. In: Kurtz, S.M. (Ed.), PEEK Biomaterials Handbook, Plastics Design Library. William Andrew Publishing, Oxford, pp. 1–7. https://doi.org/10.1016/B978-1-4377-4463-7.10001-6.
- Kusy, R.P., Whitley, J.Q., 2005. Degradation of plastic polyoxymethylene brackets and the subsequent release of toxic formaldehyde. Am. J. Orthod. Dentofac. Orthop. 127, 420–427. https://doi.org/10.1016/j.ajodo.2004.01.023.
- Lee, J.W., Buchanan, A.C., Evans, B.R., Kidder, M., 2013. Oxygenation of Biochar for Enhanced Cation Exchange Capacity, in: Lee, James W. (Ed.), Advanced Biofuels and Bioproducts. Springer, New York, NY, pp. 35–45. https://doi.org/10.1007/978-1-4614-3348-4\_4.
- Lee, H.S., Jung, S., Lin, K.-Y.-A., Kwon, E.E., Lee, J., 2023. Upcycling textile waste using pyrolysis process. Sci. Total Environ. 859, 160393 https://doi.org/10.1016/j. scitotenv.2022.160393.
- Lee, D.C., Mikulec, F.V., Korgel, B.A., 2004. Carbon Nanotube Synthesis in Supercritical Toluene. J. Am. Chem. Soc. 126, 4951–4957. https://doi.org/10.1021/ja031522s.

- Lee, L., Ou, H., Hsu, H., 2005. The experiments and correlations of the solubility of ethylene in toluene solvent. Fluid Phase Equilib. 231, 221–230. https://doi.org/ 10.1016/j.fluid.2005.02.010.
- Lettieri, P., Al-Salem, S.M., 2011. Chapter 17 Thermochemical Treatment of Plastic Solid Waste. In: Letcher, T.M., Vallero, D.A. (Eds.), Waste. Academic Press, Boston, pp. 233–242. https://doi.org/10.1016/B978-0-12-381475-3.10017-8.
- Li, J., Li, B., Zhang, X., 2002. Comparative studies of thermal degradation between larch lignin and manchurian ash lignin. Polym. Degrad. Stab. 78, 279–285. https://doi. org/10.1016/S0141-3910(02)00172-6.
- Li, L., Li, Y., Fang, Z., He, C., 2022. Study on molecular structure characteristics of natural dissolved organic nitrogen by use of negative and positive ion mode electrospray ionization Orbitrap mass spectrometry and collision-induced dissociation. Sci. Total Environ. 810, 152116 https://doi.org/10.1016/j. scitotenv.2021.152116.
- Liao, C., Li, Y., Tjong, S.C., 2020. Polyetheretherketone and Its Composites for Bone Replacement and Regeneration. Polymers 12, 2858. https://doi.org/10.3390/ polym12122858.
- Liu, Y., Chandra Akula, K., Dandamudi, P.R., K., Liu, Yingxin, Xu, M., Sanchez, A., Zhu, D., Deng, S, 2022b. Effective depolymerization of polyethylene plastic wastes under hydrothermal and solvothermal liquefaction conditions. Chem. Eng. J. 446, 137238 https://doi.org/10.1016/j.cej.2022.137238.
- Liu, X., Shan, Z., Liu, J., Xia, H., Ao, X., Zou, A., Wu, S., 2022a. Mechanical and electrical properties of additive manufactured high-performance continuous glass fiber reinforced PEEK composites. Compos. B Eng. 247, 110292 https://doi.org/10.1016/ j.compositesb.2022.110292.
- Lu, P., Huang, Q., (Thanos) Bourtsalas, A.C., Chi, Y., Yan, J., 2018. Synergistic effects on char and oil produced by the co-pyrolysis of pine wood, polyethylene and polyvinyl chloride. Fuel 230, 359–367. https://doi.org/10.1016/j.fuel.2018.05.072.
- Mamunya, Ye.P., Muzychenko, Yu.V., Pissis, P., Lebedev, E.V., Shut, M.I, 2001. Processing, Structure, and Electrical Properties of Metal-Filled Polymers. Journal of Macromolecular Science, Part B 40, 591–602. https://doi.org/10.1081/MB-100106179.
- Martin, J.P., Mccartney, S.R., Kander, R.G., 2003. An investigation of the microstructure of a cryogenically mechanically alloyed polycarbonate-poly(aryl ether ether ketone) system. J. Mater. Sci. 38, 195–200. https://doi.org/10.1023/A:1021137324461.
- Matos, M.C., Ilharco, L.M., Almeida, R.M., 1992. The evolution of TEOS to silica gel and glass by vibrational spectroscopy. Journal of Non-Crystalline Solids, Advanced Materials from Gels 147–148, 232–237. https://doi.org/10.1016/S0022-3093(05) 80622-2
- Mehmet-Alkan, A.A., Hay, J.N., 1993. The crystallinity of PEEK composites. Polymer 34, 3529–3531. https://doi.org/10.1016/0032-3861(93)90487-U.
- Mondal, M.K., Bose, B.P., Bansal, P., 2019. Recycling waste thermoplastic for energy efficient construction materials: An experimental investigation. J. Environ. Manage. 240, 119–125. https://doi.org/10.1016/j.jenvman.2019.03.016.
- Mumtaz, H., Sobek, S., Werle, S., Sajdak, M., Muzyka, R., 2023. Hydrothermal treatment of plastic waste within a circular economy perspective. Sustain. Chem. Pharm. 32, 100991 https://doi.org/10.1016/j.scp.2023.100991.
- Murthy, N.S., 2006. Hydrogen bonding, mobility, and structural transitions in aliphatic polyamides. J Polym Sci B 44, 1763–1782. https://doi.org/10.1002/polb.20833.
- Nava, D., de Parada, T.R., González, E., Boscàn, N., De La Cruz, C., 1996. An infrared spectroscopic comparison of cis- and trans-CH□CH and vinyl CH□CH2 group frequencies of some hexenes, heptenes, and stereospecific and non-stereospecific polybutadienes. Spectrochim. Acta A Mol. Biomol. Spectrosc. 52, 1201–1210. https://doi.org/10.1016/0584-8539(96)01676-5.
- Oh, K., Kim, H., Seo, Y., 2019. Effect of Diamine Addition on Structural Features and Physical Properties of Polyamide 6 Synthesized by Anionic Ring-Opening Polymerization of e-Caprolactam. ACS Omega 4, 17117–17124. https://doi.org/ 10.1021/acsomega.9b01342.
- Pamidimukkala, K.M., Kern, R.D., Patel, M.R., Wei, H.C., Kiefer, J.H., 2002. Hightemperature pyrolysis of toluene [WWW Document]. ACS Publications. https://doi. org/10.1021/i100292a034.
- Park, Y.-K., Ha, J.-M., Oh, S., Lee, J., 2021. Bio-oil upgrading through hydrogen transfer reactions in supercritical solvents. Chem. Eng. J. 404, 126527 https://doi.org/ 10.1016/j.cej.2020.126527.
- Patel, P., Hull, T.R., McCabe, R.W., Flath, D., Grasmeder, J., Percy, M., 2010. Mechanism of thermal decomposition of poly(ether ether ketone) (PEEK) from a review of decomposition studies. Polym. Degrad. Stab. 95, 709–718. https://doi.org/10.1016/ j.polymdegradstab.2010.01.024.
- Perng, L.H., Tsai, C.J., Ling, Y.C., 1999. Mechanism and kinetic modelling of PEEK pyrolysis by TG/MS. Polymer 40, 7321–7329. https://doi.org/10.1016/S0032-3861 (99)00006-3.
- Preetam, A., Jadhao, P.R., Naik, S.N., Pant, K.K., Kumar, V., 2023. Supercritical fluid technology an eco-friendly approach for resource recovery from e-waste and plastic waste: A review. Sep. Purif. Technol. 304, 122314 https://doi.org/10.1016/j.seppur.2022.122314.
- Quaid, T., Ghalandari, V., Reza, T., 2022. Effect of Synthesis Process, Synthesis Temperature, and Reaction Time on Chemical, Morphological, and Quantum Properties of Carbon Dots Derived from Loblolly Pine. Biomass 2, 250–263. https://doi.org/10.3390/biomass2040017.
- Rahman, K.M., Letcher, T., Reese, R., 2016. Mechanical Properties of Additively Manufactured PEEK Components Using Fused Filament Fabrication. Presented at the ASME 2015 International Mechanical Engineering Congress and Exposition, American Society of Mechanical Engineers Digital Collection. https://doi.org/ 10.1115/IMECE2015-52209.
- Riaz, A., Verma, D., Zeb, H., Lee, J.H., Kim, J.C., Kwak, S.K., Kim, J., 2018. Solvothermal liquefaction of alkali lignin to obtain a high yield of aromatic monomers while

- suppressing solvent consumption. Green Chem. 20, 4957–4974. https://doi.org/
- Saha, N., Banivaheb, S., Toufiq Reza, M., 2022a. Towards solvothermal upcycling of mixed plastic wastes: Depolymerization pathways of waste plastics in sub- and supercritical toluene. Energy Conversion and Management: X 13, 100158. https:// doi.org/10.1016/j.ecmx.2021.100158.
- Saha, N., Uddin, M.H., Reza, M.T., 2022b. Preliminary safety evaluation of solvothermal liquefaction of plastic wastes using toluene as solvent. Clean Techn Environ Policy 24, 801–813. https://doi.org/10.1007/s10098-021-02064-5.
- Sangon, S., Ratanavaraha, S., Ngamprasertsith, S., Prasassarakich, P., 2006. Coal liquefaction using supercritical toluene–tetralin mixture in a semi-continuous reactor. Fuel Process. Technol. 87, 201–207. https://doi.org/10.1016/j.fuproc.2005.07.007.
- Santana, A., Jesus, S., Larrayoz, M.A., Filho, R.M., 2012. Supercritical Carbon Dioxide Extraction of Algal Lipids for the Biodiesel Production. Procedia Engineering, CHISA 2012 (42), 1755–1761. https://doi.org/10.1016/j.proeng.2012.07.569.
- Santiago, C.C., Yelamanchi, B., Diosdado De la Peña, J.A., Lamb, J., Roguski, K., Turzyński, F., Faruqui, R., Choo, K., Du Plessis, A., Sillani, F., MacDonald, E., Cortes, P., 2021. Thermoplastic Extrusion Additive Manufacturing of High-Performance Carbon Fiber PEEK Lattices. Crystals 11, 1453. https://doi.org/ 10.3390/cryst11121453.
- Saxby, J.D., 1980. Atomic HC ratios and the generation of oil from coals and kerogens. Fuel 59, 305–307. https://doi.org/10.1016/0016-2361(80)90214-8.
- Scelia, R.P., Schonfeld, S.E., Donaruma, L.G., 1967. Some effects of cocatalyst structure on the anionic polymerization of e-caprolactam. II. Journal of Applied Polymer Science 11, 1299–1313. https://doi.org/10.1002/app.1967.070110726.
- Serrano, D.P., Aguado, J., Vicente, G., Sánchez, N., 2007. Effects of hydrogen-donating solvents on the thermal degradation of HDPE. J. Anal. Appl. Pyrol. 78, 194–199. https://doi.org/10.1016/j.jaap.2006.07.001.
- Seshasayee, M.S., Savage, P.E., 2020a. Oil from plastic via hydrothermal liquefaction: Production and characterization. Appl. Energy 278, 115673. https://doi.org/10.1016/j.apenergy.2020.115673.
- Shibagaki, K., Motojima, S., Umemoto, Y., Nishitani, Y., 2001. Outermost surface microstructure of as-grown, heat-treated and partially oxidized carbon microcoils. Carbon 39, 1337–1342. https://doi.org/10.1016/S0008-6223(00)00231-1.
- Singh, B., Sharma, N., 2008. Mechanistic implications of plastic degradation. Polym. Degrad. Stab. 93, 561–584. https://doi.org/10.1016/j. polymdegradstab.2007.11.008.
- Stuart, A.V., Sutherland, G.B.B.M., 2004. Effect of Hydrogen Bonding on the Deformation Frequencies of the Hydroxyl Group in Alcohols. J. Chem. Phys. 24, 559–570. https://doi.org/10.1063/1.1742546.
- Su, Y., Guo, B., Hornung, U., Dahmen, N., 2022. FeCl3-supported solvothermal liquefaction of Miscanthus in methanol. Energy 258, 124971. https://doi.org/ 10.1016/j.energy.2022.124971.
- Sung, Y.T., Han, M.S., Song, K.H., Jung, J.W., Lee, H.S., Kum, C.K., Joo, J., Kim, W.N., 2006. Rheological and electrical properties of polycarbonate/multi-walled carbon nanotube composites. Polymer 47, 4434–4439. https://doi.org/10.1016/j. polymer 2006.04.008
- Tripp, C.P., Hair, M.L., 1993. Chemical attachment of chlorosilanes to silica: a two-step amine-promoted reaction. J. Phys. Chem. 97, 5693–5698. https://doi.org/10.1021/ i100123-038
- Vicard, C., De Almeida, O., Cantarel, A., Bernhart, G., 2017. Experimental study of polymerization and crystallization kinetics of polyamide 6 obtained by anionic ring opening polymerization of  $\epsilon$ -caprolactam. Polymer 132, 88–97. https://doi.org/10.1016/j.polymer.2017.10.039.
- Wądrzyk, M., Korzeniowski, Ł., Plata, M., Janus, R., Lewandowski, M., Borówka, G., Maziarka, P., 2023. Solvothermal Liquefaction of Blackcurrant Pomace in the Water-Monohydroxy Alcohol Solvent System. Energies 16, 1127. https://doi.org/10.3390/ en16031127.
- Wan, Y., Yu, S., Jiang, S., Pei, Q., Xu, S., Cao, W., Liu, X., Lan, Y., 2021. Microscopic pyrolysis mechanism on the octyphenylsiloxane flame retarded polycarbonate by reactive molecular dynamics. J. Anal. Appl. Pyrol. 158, 105274 https://doi.org/ 10.1016/j.jaap.2021.105274.
- Wang, X., Xie, X., Sun, J., Liao, W., 2019. Effects of liquefaction parameters of cellulose in supercritical solvents of methanol, ethanol and acetone on products yield and compositions. Bioresour. Technol. 275, 123–129. https://doi.org/10.1016/j. biortech.2018.12.047.
- Wu, X.L., Huang, W.M., Ding, Z., Tan, H.X., Yang, W.G., Sun, K.Y., 2014. Characterization of the thermoresponsive shape-memory effect in poly(ether ether ketone) (PEEK). J. Appl. Polym. Sci. 131 https://doi.org/10.1002/app.39844.
- Xu, L., Huang, Z., Deng, Z., Du, Z., Sun, T.L., Guo, Z.-H., Yue, K., 2021. A Transparent, Highly Stretchable, Solvent-Resistant, Recyclable Multifunctional Ionogel with Underwater Self-Healing and Adhesion for Reliable Strain Sensors. Adv. Mater. 33, 2105306. https://doi.org/10.1002/adma.202105306.
- Yang, H.-C., Wu, Q.-Y., Liang, H.-Q., Wan, L.-S., Xu, Z.-K., 2013. Thermally induced phase separation of poly(vinylidene fluoride)/diluent systems: Optical microscope and infrared spectroscopy studies. J Polym Sci B 51, 1438–1447. https://doi.org/ 10.1002/polb.23347.
- Zakharyan, E.M., Maksimov, A.L., 2022. Pyrolysis of Polyamide-Containing Materials. Process Features and Composition of Reaction Products. Russ J Appl Chem 95, 895–928. https://doi.org/10.1134/S1070427222070011.
- Zhang, K., Schnoor, J.L., Zeng, E.Y., 2012. E-Waste Recycling: Where Does It Go from Here? Environ. Sci. Technol. 46, 10861–10867. https://doi.org/10.1021/es303166s.
- Zhang, L., Wan, C., Zhang, Y., 2009. Morphology and electrical properties of polyamide 6/polypropylene/multi-walled carbon nanotubes composites. Composites Science

- and Technology, Smart Composites and Nanocomposites Special Issue with Regular Papaers 69, 2212–2217, https://doi.org/10.1016/j.compositech.2009.06.005
- Papaers 69, 2212–2217. https://doi.org/10.1016/j.compscitech.2009.06.005.

  Zhao, S., Wang, C., Bai, B., Jin, H., Wei, W., 2022. Study on the polystyrene plastic degradation in supercritical water/CO<sub>2</sub> mixed environment and carbon fixation of polystyrene plastic in CO<sub>2</sub> environment. J. Hazard. Mater. 421, 126763 https://doi.org/10.1016/j.jhazmat.2021.126763.
- Zhao, X., Ye, L., 2011. Structure and mechanical properties of polyoxymethylene/multi-walled carbon nanotube composites. Compos. B Eng. 42, 926–933. https://doi.org/
- 10.1016/j.compositesb.2011.01.002.
   Zuev, V.V., Ivanova, Y.G., 2012. Mechanical and electrical properties of polyamide-6-based nanocomposites reinforced by fulleroid fillers. Polym. Eng. Sci. 52, 1206–1211. https://doi.org/10.1002/pen.22188.